Materials Horizons

Accepted Manuscript

ROYAL SOCIETY OF CHEMISTRY

rsc.li/materials-horizons

Journal Name

RSCPublishing

COMMUNICATION

Photoswitching between black and colourless spectra exhibits resettable spatiotemporal logic†

Cite this: DOI: 10.1039/x0xx00000x

Yue Wu,[ab‡] Zhiqian Guo,[a‡] Wei-Hong Zhu,*[a] Wei Wan,[b] Junji Zhang,[a] Wenlong Li,[a] Xin Li,[c] He Tian[a] and Alexander D. Q. Li*[b]

Received 00th January 2012,
Accepted 00th January 2012

DOI: 10.1039/x0xx00000x

www.rsc.org/

Logic is the key to computing. Traditionally, logic devices have been fabricated by the top-down approach, whose dimensions are drastically limited. The ultimate goal is to use molecular tailorability to design logics from the "bottom-up" approach. Here we report an unprecedented photochromic molecule that undergoes unimolecular logic switching when excited anywhere in the entire UV-visible spectrum, thus a bottom-up, all-photonic, molecular logic gate. Specifically, these molecular photonic logics embedded in the polymer thin films function as "AND" or "OR" gate at different temporal responses. To achieve high information-processing density, moreover, a ternary flip-flap-flop gate is realized in the molecular logic because the fact that this photochromic molecule can be photoswitched anywhere in its UV-vis spectrum enabled three different lasers (532, 473, and 561 nm) as the inputs to deliver the complex logic optical outputs.

Logic functions as the brain of modern computers.[1-5] Although electronic logic circuits have revolutionized many aspects of our life, the top-down approach clearly has fundamental limitations in device dimensions.[6-9] At the top of agenda is to develop emerging logic materials, whereby molecular computing has been proved as the appropriate "bottom-up" candidate with its own potential advantages, especially the ability to operate in much smaller nanoscale.[10] Since the first molecular AND gate was demonstrated in 1993,[11] logic gates,[12-18] molecular memory elements,[19-25] optical information encoding,[26-29] and even biological logics[30-32] have been reported. Up to now, successful molecular logic gates are mainly demonstrated in solution, using concentrated reactants as inputs and specific products as outputs, usually with colour changes or other easily discernable phenomena.[3] However, logic gates in solutions are more a concept than a real-world technological application. Because solution logics consume massive chemicals, thus compromising their operations and reversibility,[13] solid devices are more desirable. Yet, molecular logic devices operating in solid state are still challenging and considered as the bottleneck in the further advancement of the bottom-up approach. Accordingly, it is rather significant to provide a route towards all-photonic, chemical-waste free, solid-state logic.[33-36]

Although many physical/chemical properties can be photo-switched ON or OFF,[22,37-41] photochromism remains as the popular mechanism in logic operation,[12-14] especially for their potential in constructing all-photonic logic gates.[42-44] Because light is capable of processing huge amount of information simultaneously, solid-state molecular logics using light as inputs and outputs not only can be ultra-fast, but also avoid making physical contacts. Here, we report an unprecedented, photochromic bisthiazolethene system (**BTA**, Fig. 1a), whose absorption covers the entire UV-visible region, thus responding to optical encoding throughout the spectrum. Furthermore, the kinetics from the closed form ***c*-BTA** to the open form **BTA** exhibits different ring-opening photoreaction rates when different visible lasers (532, 473, or/and 561 nm) are used. By taking full advantage of the whole broad spectral responses and their different photochemical kinetics, we have successfully constructed all-photonic thin-film logic gates using ***c*-BTA/BTA** as the photoactive medium to perform accurate, controllable and spatiotemporal logic operations using non-invasive light remotely.

Photoswitching of bisthiazolethene (**BTA**, Fig. 1a) reveals a radical departure from the photochromic compounds known so far- the closed form (***c*-BTA**) absorbs over the entire UV-visible spectrum! The open form (**BTA**) is colourless, while the closed form, which was obtained upon 302-nm irradiation (Fig. 2a), is completely black. Two well-defined isosbestic points appeared at 266 and 313 nm, respectively, suggesting a 1:1 conversion between **BTA** and ***c*-BTA**. The photostationary state (**PSS**) was reached within only 54 s upon irradiating **BTA** at 302 nm (1 mW; concentration: 20 μM). Conversely, visible light irradiation on the photochemically generated **PSS** triggered the back conversion to its original colourless open form **BTA** (Fig. 2a). The ring-open form **BTA** exhibits weak fluorescence while the corresponding **PSS** has essentially no emission (Fig. S1 in ESI†). Interestingly, unlike other typical photochromic compounds, **c-BTA** has two absorption bands that have just the right positions (426 and 572 nm) and bandwidth to completely black out the whole spectrum.[45-47] The net result of

reversible black-and-white interconversion, which was underpinned by the photochemical switching between ring-open and ring-closed forms, has great potential applications in optical limiting protection and digital logic operation.[48]

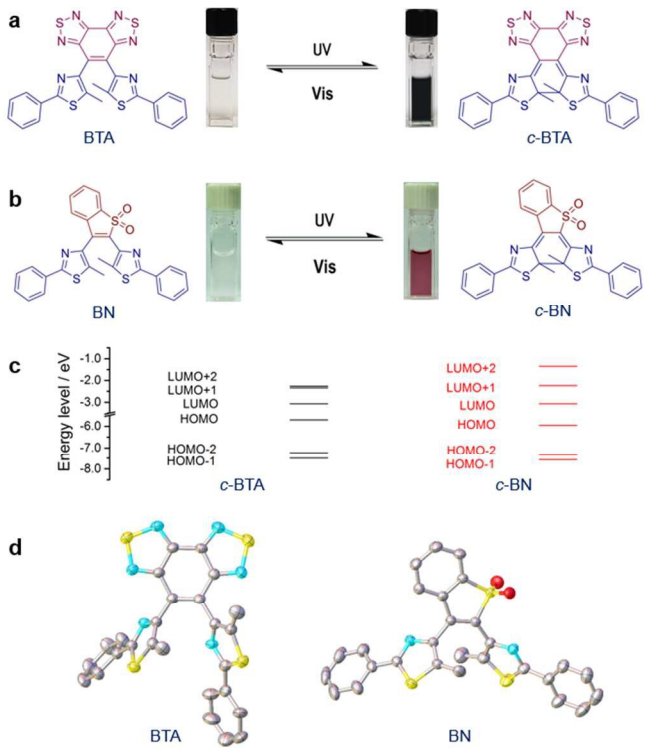

Fig. 1 Photochromic contrast between black **c-BTA** and red **c-BN**. (**a**) Reversible UV and Visible light shuttle **BTA** (colourless) and c-BTA (black) back and forth; (**b**) Reversible UV and Visible light also interconverts **BN** and ***c*-BN** reversibly; (**c**) Energy levels of frontier molecular orbitals of compounds ***c*-BTA** and ***c*-BN**. (**d**) ORTEP representation of X-ray single-crystal structures of **BTA** and **BN** in the open states drawn with 50% probability from front and top view (S: yellow; N: blue; C: grey). Detailed data of **BTA** including packing diagrams can be found in ESI†, and detailed data of **BN** could be found in reference 47.

To unveil the "blackout" mechanism created by ***c*-BTA**, molecular orbital calculations were carried out along with a normal photochromic compound **BN**[49] (Fig. 1b) as a reference. Like a typical photochromic compound, colourless **BN** undergoes ring closure photo-cyclization to form red-colour ***c*-BN** that shows a characteristic, photochromic absorption. The LUMO of the two compounds are on the same energy level (-3.07 eV); however, ***c*-BTA** has a higher HOMO and a lower LUMO+1 when compared with ***c*-BN**, and these distinguishing characters are the origin of blackout mechanism of the whole spectrum. First, the experimentally observed absorption band of ***c*-BTA** at 572 nm arises from HOMO→LUMO transition, which only locally excites the closed-ring diarylethene unit (Tables S1 and S2†). Second, the absorption band of ***c*-BTA** at 426 nm arises from HOMO→LUMO+1 and HOMO→LUMO+2 transitions with similar excitation energies due to close arrangements of the LUMO+1 and LUMO+2 energetically. These two transitions, particularly the HOMO→LUMO+1 transition, reveal strong intramolecular charge transfer from the closed diarylethene ring to the electron-withdrawing benzobisthiadiazole bridge. Therefore, the three transitions from HOMO to LUMO, LUMO+1 and LUMO+2 contribute to the observed visible spectrum of ***c*-BTA** (Fig. 2a) and cause the blackout phenomenon. Comparatively, the excitation energy required for HOMO→LUMO+1 transition in ***c*-BN** is 3.0 eV, thus placing the absorption in the near UV region. As a result, only one main peak is observed in the region of 400-600 nm, which corresponds to the HOMO → LUMO transition mostly localized within the closed diarylethene ring (Table S2†). The LUMO+2 of ***c*-BN** is localized on the oxidized benzothiophene bridge with a much higher energetic level, and accordingly the HOMO→LUMO+2 transition contributes to absorption in the UV region. In single crystals, **BN** adopts an anti-parallel conformation while **BTA** exhibits a parallel conformation (Fig. 1d, Tables S3, S4 and S5†). Because solid crystals limit group rotation, the parallel conformation does not meet the prerequisites for solid-state photochromic reaction,[48] and thus **BTA** crystals exhibit no colour change upon UV irradiation.

Alternating irradiation with UV (365 nm) and visible light (> 510 nm) toggled the molecular photoswitch repeatedly between ring-open **BTA** and ring-closed form ***c*-BTA** with good fatigue resistance and reversibility (Fig. 2b). Conversion ratio from the ring-open form to the ring-closed form was as high as 91% based on calculations via absorption spectra (Fig. S2 †). Unlike many well-known photochromisms,[51-53] ***c*-BTA** possesses an excellent thermal stability—a desired feature for logic operation and does not undergo thermal cyclo-reversion as demonstrated by the constant absorbance values at different wavelengths of 419, 494, and 572 nm (Fig. 2c). As a result, the black closed form was easily synthesized photochemically and conveniently purified by traditional column chromatography. Interestingly, when the photo-reversion efficiencies (***c*-BTA** to **BTA**) at various wavelengths were tested, different photoreaction rate constants were observed when the same PSS was irradiated with different lasers (473, 532 and 561 nm; Figs. 2d and 2e); their rate constants (k) were 1.54×10^{-2} s^{-1}, 6.66×10^{-3} s^{-1}, and 2.52×10^{-2} s^{-1} for 473-nm (0.38 mW mm^{-2}, A_{max} is 0.125 at 473 nm), 532-nm (0.19 mW mm^{-2}, A_{max} is 0.159 at 532 nm), and 561-nm (0.38 mW mm^{-2}, A_{max} is 0.196 at 561 nm) lasers, respectively. Obviously, different power density of 473-, 532-, and 561-nm lasers might induce ring-open reaction with different rate constant. Notably, the rate constant k increased to 3.94×10^{-2} s^{-1} upon combining 473-nm and 561-nm lasers together.

In electro-optical modulation, an electric field applied perpendicular to the light beam travelling in a nonlinear medium imparts modulation on the output light signals. For example, a modulated electric field can encode its signals using Mach-Zehnder device to shift the phase of the light beam that is traveling through it. Instead of an electric field, here four different laser beams (473, 532, 561, and 375 nm) were used to modulate and reset the relative amount of the **BTA** and ***c*-BTA** in a polylactic acid (PLA) thin film initially containing 5 % w/w of **BTA** (Figs. S3 and S4). Because the resulting ***c*-BTA/BTA** film has opaque and transparent bistable states, it in turn modulates the signal light beam traveling orthogonally with respect to the lasers. In such an all-optical system, in which light modulates the medium and the medium further encodes light signals, the 375-nm laser resets the open form **BTA** to the closed form ***c*-BTA**, whereas the 473, 532, and 561-nm lasers modulate the thin film optical properties by photoswitching various amount of the closed form back to the open form to impart logic operations. The photoswitchable thin film was placed at a 45° incident angle with respect to the

modulating laser beams and a 45° incident angle with respect to the input light as well as the output optical pulses (Fig. 3a).

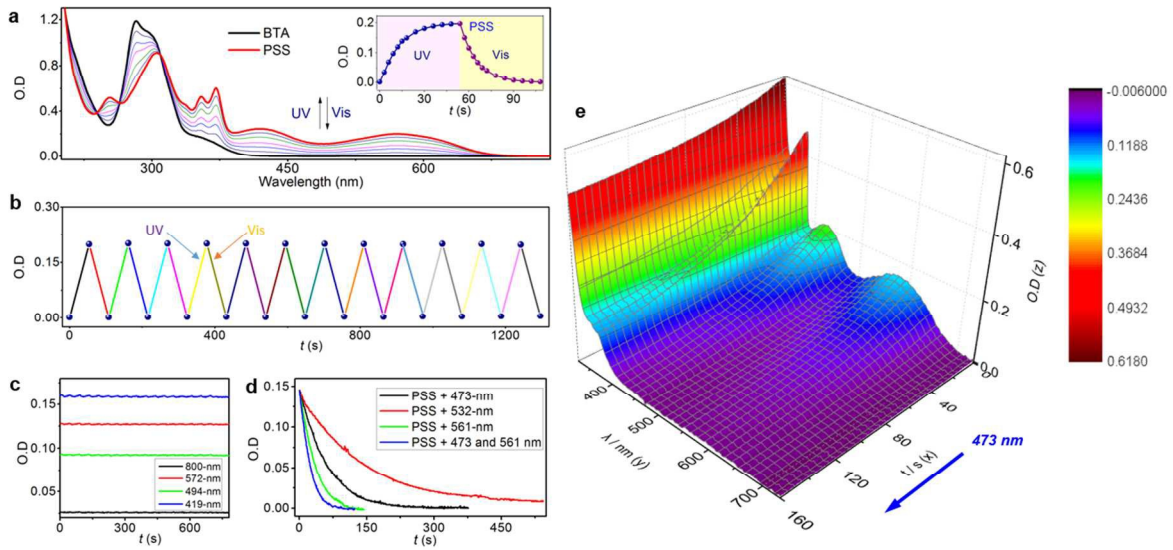

Fig. 2 Black-to-colourless photoreactions have different rate constants at different wavelengths. (a) Photoswitching from open form to **PSS** (2×10^{-5} M, CH_3CN) upon 302-nm light irradiation, and reversible photoswitching from **PSS** to open form upon > 510-nm irradiation. Inserts: photoswitching kinetics measured at 572 nm as a function of irradiation time. (b) Alternating between UV (365 nm) and visible (> 510 nm) light photoswitches open form and closed form back and forth, demonstrating good fatigue resistance and reversibility. (c) Absorbance values of **BTA** monitored at 419, 494, 572 nm and room temperature in CH_3CN after it reaches the **PSS** under UV action indicate no reversal reaction after 780 minutes, confirming that ***c*-BTA**, like **BTA**, is thermally stable. (d) Reversible photoswitching from **PSS** to **BTA** (2.0×10^{-5} M, $CHCl_3$) upon 473-nm (black line), 532-nm (red line), 561-nm (green line), and the combination of 473-nm and 561-nm laser (blue line) irradiation. (e) Three-dimensional (3D) plot that relates optical density (z-axis) to time (x-axis) and wavelength (y-axis) reveals the absorption dynamics upon irradiation at 473 nm laser, as the ring-closed (***c*-BTA**) is photochemically converted to the ring-open (**BTA**) form.

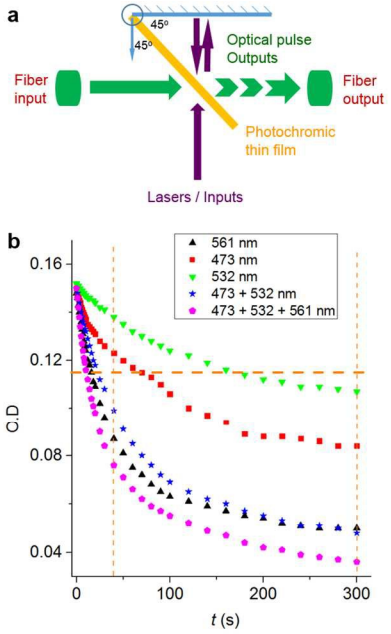

Fig. 3 The ***c*-BTA↔BTA** photochromic system orthogonally modulated for regulating output signals. (**a**) The photo-optical modulation system illustrates that modulation beams (violet arrows) change the continuous white light traveling orthogonally into modulated beam (green arrows); both have an incident angle of 45° with respect to the photoswitching thin film containing BTA and c-BTA. (**b**) After resetting by the 365-nm laser (OD = 0.15 at 579 nm), the PSS (closed form) was driven back to the open form using 532-nm laser (green dot), 473-nm laser (red dot), 561-nm laser (black dot), the combination of 473- and 532-nm lasers (blue dot), and the combination of 473-, 532-, and 561-nm lasers (pink dot), respectively. Film thickness: 15 μm; BTA/PLA = 5% w/w.

After the 375-nm laser resets the thin film to the "opaque" state, various other lasers or their combinations were used to photoswitch the medium toward the transparent direction. Distinct reaction rate constants were observed when different lasers (561, 473 and 532 nm) or their combinations were used as the modulation beam (Fig. 3b). Specifically, the rate constants (k) were 1.4×10^{-2} s^{-1} (473 nm, 3.8×10^{-2} mW mm^{-2}), 2.9×10^{-3} s^{-1} (532 nm, 1.9×10^{-2} mW mm^{-2}), 2.8×10^{-2} s^{-1} (561 nm, 3.8×10^{-2} mW mm^{-2}), 2.6×10^{-2} s^{-1} (473 + 532 nm), and 3.2×10^{-2} s^{-1} (473 + 532 + 561 nm). These results reveal appreciable disparity among the rate constants, which can be exploited to perform logic operations.

The well-behaved ***c*-BTA→BTA** photoswitching was fabricated into thin-film devices for logic computing. Contrasted to established logic gates that use chemical species as inputs, all-photonic logics employ laser beams as inputs, thus avoiding manipulating complicated chemicals. While the laser "on" and "off" were used to define the input as "1" and "0", the absorbance change (ΔA) as measured by the orthogonally passing beam defines the output. Fig. 4a depicts that the **BTA** device functions as AND / OR logic gates, with the threshold of the output absorbance change set as 0.035. According to Fig. 3b, when both 532-nm and 473-nm lasers are turned on (Input 1 = 1 and Input 2 = 1), the AND gate was realized by measuring the 579-nm ΔA *value* at 40 s, which is defined as the Output 1 (Fig. 4a). At 40 s only when both In1 (532 nm) and In2 (473 nm) are on (1,1), Output 1 (ΔA = 0.051) is greater than the threshold ΔA that is set as 0.035 and yields true logic

(Output 1 = 1). In contrast, the OR gate was defined as the 579-nm Δ*A value* at 300 s, which was assigned as Output 2. The "true" state of this OR gate can be either triggered by either In1 (532 nm) or In2 (473 nm) signal (Fig. 4a).

Intriguingly, the same ***c*-BTA → BTA** photoswitching device functions as AND gate at 40 s and as OR gate at 300 s based on the Δ*A value* at 579 nm. This endows an all-photonic logic gate with the temporal characteristic, and the logic gate based on ***c*-BTA** film can be switched between AND and OR gates simply by reading the output at different time. Thus, with the same inputs, ***c*-BTA/BTA** photochromic system performs different logic function at different irradiation time, producing a specific temporal logic. Because the devices are solid state rather than solutions, only those regions illuminated experienced photoswitching or logic operations, thus offering spatiotemporal logics.

In addition to two-input logic gates, complicated three-terminal logic gates have also been developed while sequentially combining the AND and OR computing. According to Fig. 3b, the effect of 561-nm irradiation almost equals to that of the combination of 532 nm and 473 nm irradiation, thus an AND gate and an OR gate combined logic can be constructed. As shown in Fig. 4b, this complex logic gate has three inputs, In1 (473 nm laser), In2 (532 nm laser) and In3 (561 nm). At 40 s, when In1 and In2 both are on or when In3 is on, the output will be over the threshold, yielding a true result, Output 1 = 1. Furthermore, this AND gate (reading at 40 s) becomes OR gate when reading at 300 s; thus Output 2 is a combined logic from two OR gates.[42] For this double OR logics, only when all three inputs are false (0), the output will be false (0). Otherwise, the output is true (1).

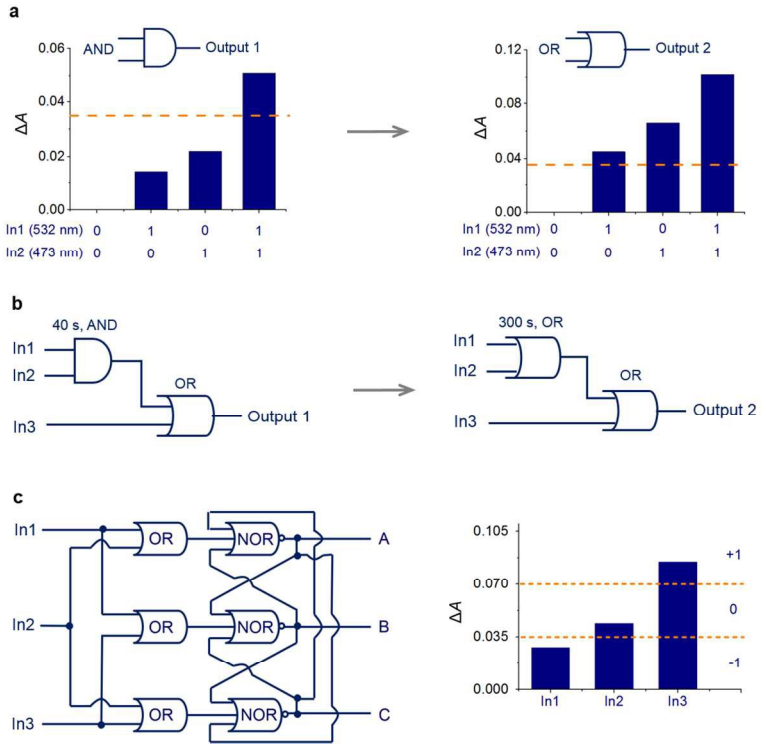

In1 532 nm	In2 473 nm	AND gate Output 1 ΔA 40 s	OR gate Output 2 ΔA 300 s
0	0	0	0
1	0	0	1
0	1	0	1
1	1	1	1

In1 532 nm	In2 473 nm	In3 561 nm	Output 1 ΔA 40 s	Output 2 ΔA 300 s
0	0	0	0	0
1	0	0	0	1
0	1	0	0	1
1	1	0	1	1
0	0	1	1	1
1	0	1	1	1
0	1	1	1	1
1	1	1	1	1

Inputs			Output ΔA			
In1 532 nm	In2 473 nm	In3 561 nm	A	B	C	Overall
0	0	0	original state			
1	0	0	0	0	1	-1
0	1	0	0	1	0	0
0	0	1	1	0	0	+1

Fig. 4 Spatiotemporal logics. (**a**) Schematic diagram of AND or OR logic-gate response using 532 nm laser (Input 1) and 473 nm laser (Input 2) as inputs. Absorption change Δ*A* of 40 s is set to be Output 1, and Δ*A value* at 300 s is set to be Output 2, and their truth tables is shown on the right. As time elapses, AND gate (40 s) will switch to OR gate (300 s). (**b**) The three-input complementation of AND and OR gate response of 532 nm laser (In1), 473 nm laser (In2) and 561 nm laser (In3), Δ*A* of 40 and 300 s are set as Output 1 and Output 2 respectively, their corresponding truth tables are on the right. (**c**) Schematic of the flip-flap-flop logic gate (OR and NOR)51 that responds to various inputs of In1 (532 nm), In2 (473 nm) or In3 (561 nm). Various inputs are shown in the table on the left: note that only one input at a time. The 100-s Δ*A value* functions for the flip-flap-flop logic-gate when the thresholds are set to be 3.5×10^{-2} and 7.0×10^{-2} to distinguish -1, 0, and +1. The output +1 corresponds to ΔA over 7.0×10^{-2}; 0 in between 3.5×10^{-2} and 7.0×10^{-2}; -1 with $\Delta A < 3.5 \times 10^{-2}$ as shown in the characteristic truth table on the right.

To meet the demand of ever-increasing information density, a ternary system for transferring and storing information is highly desirable because it is approximately 1.6 times more efficient than that of the binary system. Because of this, we used the ***c*-BTA** photoswitching properties to design and construct a resettable flip-flap-flop logic gate.[54] Generally, the flip-flap-flop contains two linked units: three OR logic gates (first unit) convert the input sequence from In1, In2, and In3 into an appropriate input for the three cross-coupled NOR gates (second unit), which import the memory of the given inputs (Fig. 4c). The photoswitching kinetics of ***c*-BTA** cyclo-reversion has three distinct rate constants under the three input lasers: the 561-nm laser triggered the fastest cyclo-reversion (Δ*A* = 0.085); the 532 nm laser triggered the slowest reversible reaction (Δ*A* = 0.028); the 473-nm laser triggered a response in between the 561- and 532-nm lasers (Δ*A* = 0.044). This way, when In1 (532 nm laser) is active, the cyclo-reversion rate is the slowest and the system is in state -1 (output string 0 0 1). On the contrary, while In3 (561 nm laser) is applied, the cyclo-reversion rate is the fastest and the system is in state +1 (output string 1 0 0). Moreover, while In2 (473 nm laser) is addressed, the reaction rate is in-between 561 and 532 nm, so remains in state 0 (output string 0 1 0). The characteristic truth table for the flip-flap-flop logic is shown in Fig. 4c. Furthermore, this logic can be reset by

10-s 375-nm UV laser irradiation, which restore the system to the original PSS state and ready for the next round information input.

In summary, contrary to classic photochromism, a rare photochromic ***c*-BTA**, which absorbs in the entire spectrum, was demonstrated. The unprecedented black-absorption originates mainly from three transitions from HOMO to LUMO, LUMO+1 and LUMO+2, which contribute to the two observed absorption bands covering from 350 to 650 nm. Because of this, the photochromic system ***c*-BTA/BTA** can be modulated by many wavelengths (lasers), with good fatigue resistance and high thermal stability. Most importantly, photo-cycloreversion reaction rates of ***c*-BTA** depend on the laser wavelengths. This striking feature enabled a series of solid-state logic devices that have spatiotemporal logics. Furthermore, the intrinsic photo-responsiveness of ***c*-BTA** to 532, 473, and 561 nm lasers allows the design of a base-three logic gate that can expand into ternary logics to meet future need of high-density information processing and computing.

The present study has introduced all-photonic, solid-state logic gates that use the spatiotemporal responses of photochromic ***c*-BTA/BTA** system to create logic operations. This unique molecular design of solid-state logic gates would provide a novel method for future practical logic device fabrication. Switchable and inter-convertible Boolean logic unit may be assembled by appropriate combination of photo-responsive molecular components with time-dependent excitation. These solid logics overcome the limitations of solution media, thus one step closer to future information or computation devices.

Acknowledgements

This work was supported by National 973 Program (2013CB733700), NSFC for Creative Research Groups (21421004) and Distinguished Young Scholars (21325625), NSFC/China, Oriental Scholarship, Shanghai Pujiang Program (13PJD010), Fok Ying Tong Education Foundation (142014), Fundamental Research Funds for the Central Universities (222201313010, WK1314008 and WJ1416005), Scientific Committee of Shanghai (15XD1501400), and National Science Foundation (CHE-1213358).

Notes and references

[a]Key Laboratory for Advanced Materials and Institute of Fine Chemicals, Shanghai Key Laboratory of Functional Materials Chemistry, East China University of Science and Technology, Shanghai 200237, China. E-mail: whzhu@ecust.edu.cn.

[b]Department of Chemistry, Washington State University, Pullman, 99164, USA. E-mail: dequan@wsu.edu

[c]Division of Theoretical Chemistry and Biology, School of Biotechnology, KTH Royal Institute of Technology, SE-10691 Stockholm, Sweden.

‡ Contributed equally

† Electronic Supplementary Information (ESI) available: Synthetic routes for **BTA** and their optimized ground-state geometry. See DOI: 10.1039/c000000x/

1. M. Ben-Ari, Mathematical Logic for Computer Science. *Prentice Hall* (1993)
2. A. P. de Silva, *Nature*, 2008, **454**, 417-418.
3. A. P. de Silva, Molecular logic-based computation. *RSC Publishing* (2013).
4. K. Szacilowski, *Chem. Rev.*, 2008, **108**, 3481-3548.
5. J. Andréasson and U. Pischel, *Chem. Soc. Rev.*, 2010, **39**, 174-188.
6. M. A. Reed and J. M. Tour, *Sci. Am.*, 2000, **282**, 86-93.
7. J. M. Tour, *Acc. Chem. Res.*, 2000, **33**, 791-804.
8. R. W. Keyes, *Proc. IEEE*, 2001, **89**, 227-239.
9. *International Technology Roadmap for Semiconductors (ITRS 2005 Edition)*, http://www.itrs.net/Links/2005ITRS/Home2005.htm.
10. R. Ballardini, P. Ceroni, A. Credi, M. T. Gandolfi, M. Maestri, M. Semararo, M. Venturi and V. Balzani, *Adv. Funct. Mater.*, 2007, **17**, 740-750.
11. A. P. de Silva, H. Q. N. Gunaratne and C. P. McCoy, *Nature*, 1993, **364**, 42-44.
12. X. J. Jiang and D. K. P. Ng, *Angew. Chem. Int. Ed.*, 2014, **54**, 10481-10484.
13. S. J. Chen, Y. H. Yang, Y. Wu, H. Tian and W. H. Zhu, *J. Mater. Chem.*, 2012, **22**, 5486-5494.
14. U. Pischel, *Angew. Chem. Int. Ed.*, 2007, **46**, 4026–4040.
15. M. Amelia, M. Baroncini and A. Credi, *Angew. Chem. Int. Ed.*, 2008, **47**, 6240–6243.
16. S. Kou, H. N. Lee, D. Van Noort, K. M. K. Swamy, S. H. Kim, J. H. Soh, M. Lee, S. W. Nnam, J. Yoon and S. Park, *Angew. Chem. Int. Ed.*, 2008, **47**, 872–876.
17. Z. Q. Guo, W. H. Zhu, L. J. Shen and H. Tian, *Angew. Chem. Int. Ed.*, 2007, **46**, 5549–5553.
18. D. Margulies, G. Melman and A. Shanzer, *Nat. Mater.*, 2005, **4**, 768-771.
19. H. B. Sun, S. J. Liu, W. P Lin, K. Y. Zhang, W. Lv, X. Huang, F. W. Huo, H. R. Yang, G. Jenkins, Q. Zhao and W. Huang, *Nat. Commun.*, 2014, **5**, 3601.
20. G. de Ruiter, E. Tartakovsky, N. Oded and M. E. van der Boom, *Angew. Chem. Int. Ed.*, 2010, **49**, 169-172.
21. J. Kärnbratt, M. Hammarson, S. M. Li, H. L. Anderson, B. Albinsson and J. Andréasson, *Angew. Chem. Int. Ed.*, 2010, **49**, 1854-1857.
22. M. Irie, *Chem. Rev.*, 2000, **100**, 1685-1716.
23. X. F. Guo, D. Q. Zhang, Y. Gui, M. X. Wan, Y. Q. Liu and D. B. Zhu, *Adv. Mater.*, 2004, **16**, 636-640.
24. T. Fukaminato, T. Doi, N. Tamaoki, K. Okuno, Y. Ishibashi, H. Miyasaka and M. Irie, *J. Am. Chem. Soc.*, 2011, **133**, 4984-4990.
25. M. Berberich, A. M. Krause, M. Orlandi, F. Scandola and F. Würthner, *Angew. Chem. Int. Ed.*, 2008, **47,** 6616-6619.
26. Y. Wu, Y. S. Xie, Q. Zhang, H. Tian, W. H. Zhu and A. D. Q Li, *Angew. Chem. Int. Ed.*, 2014, **53**, 2090-2094.
27. J. Yoon, *Angew. Chem. Int. Ed.*, 2014, **53**, 6600-6601.
28. M. Irie, T. Fukaminato, T. Sasaki, N. Tamai and T. Kawai, *Nature*, 2002, **420**, 759-760.
29. A. Kishimura, T. Yamashita, K. Yamaguchi and T. Adia, *Nat. Mater.*, 2005, **4**, 546-549.
30. M. Ikeda, T. Tanida, T. Yoshii, K. Kurotani, S. Onogi, K. Urayama and I. Hamachi, *Nat. Chem.*, 2014, **6**, 511-518.
31. X. Chen, Y. F. Wang, Q. Liu, Z. Z. Zhang, C. H. Fan and L. He, *Angew. Chem. Int. Ed.*, 2006, **45**, 1759-1762.
32. F. Lohmann, J. Weigandt, J. Valero and M. Famulok, *Angew. Chem. Int. Ed.* 2014, **53**, 10372-10376.

33. E. H. Witlicki, C. Johnsen, S. W. Hansen, D. W. Silverstein, V. J. Bottomley, J. O. Jeppesen, E. W. Wong, L. Jensen and A. H. Flood, *J. Am. Chem. Soc.*, 2011, **133**, 7288−7291.
34. Y. Liu, F. Qin, Z. M. Meng, F. Zhou, Q. H. Mao and Z. Y. Li, *Optics Express*, 2011, **19**, 1945-1953.
35. S. Silvi, E. C. Constable, C. E. Housecroft, J. E. Beves, E. L. Dunphy, M. Tomasulo, F. M. Raymo and A. Credi, *Chem. Eur. J.*, 2009, **15**, 178-185.
36. M. Bälter, S. M. Li, J. R. Nilsson, J. Andréasson and U. Pischel, *J. Am. Chem. Soc.*, 2013, **135**, 10230-10233.
37. W. Szymański, J. M. Beierle, H. A. V. Kistemaker, W. A. Velema and B. L. Feringa, *Chem. Rev.*, 2013, **113**, 6114–6178.
38. J. J. Zhang, Q. Zou and H. Tian, *Adv. Mater.*, 2013, **25**, 378−399.
39. A. M. Asadirad, S. Boutault, Z. Erno and N. R. Branda, *J. Am. Chem. Soc.*, 2014, **136**, 3024−3027.
40. A. Spangenberg, R. Métivier, J. Gonzalez, K. Nakatani, P. Yu, M. Giraud, A. Léaustic, R. Guillot, T. Uwada and T. R. Asahi, *Adv. Mater.*, 2004, **21**, 309−313.
41. W. H. Zhu, Y. H. Yang, R. Métivier, Q. Zhang, R. Guillot, Y. S. Xie, H. Tian and K. Nakatani, *Angew. Chem. Int. Ed.*, 2011, **50**, 10986−10990.
42. J. Andréasson, U. Pischel, S. D. Straight, T. A. Moore, A. L. Moore and D. Gust, *J. Am. Chem. Soc.*, 2011, **133**, 11641−11648.
43. S. D. Straight, P. A. Liddell, Y. Terazona, T. A. Moore, A. L. Moore and D. Gust, *Adv. Funct. Mater.*, 2007, **17**, 777-785.
44. F. B. Meng, Y. M. Hervault, Q. Shao, B. H. Hu, L. Norel, S. Rigaut and X. D. Chen, *Nat. Commun.*, 2014, **5**, 3023.
45. Z. Y. Tian, W. W. Wu, W. Wan and A. D. Q. Li, *J. Am. Chem. Soc.*, 2011, **133**, 16092-16100.
46. Y. Zou, T. Yi, S. Z. Xiao, F. Y. Li, C. Y. Li, X. Gao, J. C. Wu, M. X. Yu and C. H. Huang, *J. Am. Chem. Soc.*, 2008, **130**, 15750−15751.
47. C. T. Poon, W. H. Lam and V. W. W. Yam, *J. Am. Chem. Soc.*, 2011, **133**, 19622-19625.
48. Y. Chen, M. Hanack, Y. Araki and O. Ito, *Chem. Soc. Rev.*, 2005, **34**, 517-529.
49. Y. Wu, S. J. Chen, Y. H. Yang, Q. Zhang, Y. S. Xie, H. Tian and W. H. Zhu, *Chem. Commun.*, 2012, **48**, 528-530.
50. S. Kobatake, K. Uchida, E. Tsuchida and M. Irie, *Chem. Commun.*, 2002, 2804-2805.
51. W. H. Zhu, L. W. Song, Y. H. Yang and H. Tian, *Chem. Eur. J.*, 2012, **18**, 13388-13394.
52. L. Y. Zhu, M. Q. Zhu, J. K. Hurst and A. D. Q. Li, *J. Am. Chem. Soc.*, 2005, **127**, 8968-8970.
53. Z. Y. Tian, W. W. Wu, W. Wan and A. D. Q. Li, *J. Am. Chem. Soc.*, 2011, **133**, 16092-16100.
54. G. de Ruiter, L. Motiei, J. Choudhury, N. Oded and M. E. van der Boom, *Angew. Chem. Int. Ed.*, 2010, **49**, 4780-4783.

Photoswitching between black and colourless spectra exhibits resettable spatiotemporal logic

Yue Wu, Zhiqian Guo, Wei-Hong Zhu,* Wei Wan, Junji Zhang, Wenlong Li, Xin Li, He Tian and Alexander D. Q. Li*

All-photonic, solid-state logic gates are constructed with exploting the spatiotemporal responses of photochromic ***c*-BTA**/**BTA** system to create logic operations.

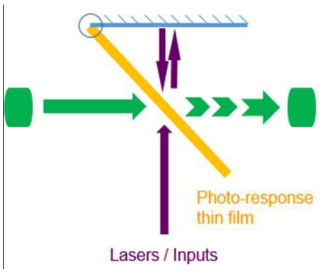

Conceptual insights

Switchable and inter-convertible Boolean logic unit can be assembled by appropriate combination of photo-responsive molecular components with time-dependent excitation. Up to date, molecular logic devices operating in solid state are still considered as the bottleneck in the further advancement of the bottom-up approach. The present study has introduced all-photonic, solid-state logic gates that use the spatiotemporal responses of photochromic system with broad absorption response to create logic operations. This unique molecular design of solid-state logic gates would provide a novel method for future practical logic device fabrication.